doi:10.1093/brain/awt276 Brain 2013: 136; 3796–3808 | 3796

BRAIN
A JOURNAL OF NEUROLOGY

Ictal high frequency oscillations distinguish two types of seizure territories in humans

Shennan A. Weiss,[1] Garrett P. Banks,[2] Guy M. McKhann Jr,[2] Robert R. Goodman,[2] Ronald G. Emerson,[1,3] Andrew J. Trevelyan[4,†] and Catherine A. Schevon[1,†]

1 Department of Neurology, Columbia University, New York, NY, USA
2 Department of Neurological Surgery, Columbia University, New York, NY, USA
3 Hospital for Special Surgery, Cornell University, New York, NY, USA
4 Institute of Neuroscience, Newcastle University, Medical School, Framlington Place, Newcastle upon Tyne, NE2 4HH, UK

[†]These authors contributed equally to this work.

Correspondence to: Catherine Schevon,
710 West 168th Street,
New York,
NY 10032 USA
E-mail: cas2044@columbia.edu

High frequency oscillations have been proposed as a clinically useful biomarker of seizure generating sites. We used a unique set of human microelectrode array recordings (four patients, 10 seizures), in which propagating seizure wavefronts could be readily identified, to investigate the basis of ictal high frequency activity at the cortical (subdural) surface. Sustained, repetitive transient increases in high gamma (80–150 Hz) amplitude, phase-locked to the low-frequency (1–25 Hz) ictal rhythm, correlated with strong multi-unit firing bursts synchronized across the core territory of the seizure. These repetitive high frequency oscillations were seen in recordings from subdural electrodes adjacent to the microelectrode array several seconds after seizure onset, following ictal wavefront passage. Conversely, microelectrode recordings demonstrating only low-level, heterogeneous neural firing correlated with a lack of high frequency oscillations in adjacent subdural recording sites, despite the presence of a strong low-frequency signature. Previously, we reported that this pattern indicates a failure of the seizure to invade the area, because of a feedforward inhibitory veto mechanism. Because multi-unit firing rate and high gamma amplitude are closely related, high frequency oscillations can be used as a surrogate marker to distinguish the core seizure territory from the surrounding penumbra. We developed an efficient measure to detect delayed-onset, sustained ictal high frequency oscillations based on cross-frequency coupling between high gamma amplitude and the low-frequency (1–25 Hz) ictal rhythm. When applied to the broader subdural recording, this measure consistently predicted the timing or failure of ictal invasion, and revealed a surprisingly small and slowly spreading seizure core surrounded by a far larger penumbral territory. Our findings thus establish an underlying neural mechanism for delayed-onset, sustained ictal high frequency oscillations, and provide a practical, efficient method for using them to identify the small ictal core regions. Our observations suggest that it may be possible to reduce substantially the extent of cortical resections in epilepsy surgery procedures without compromising seizure control.

Keywords: epilepsy surgery; seizure localization; human microelectrode recordings; high frequency oscillations
Abbreviations: HFO = high frequency oscillation; PLHG = phase-locked high gamma

Received May 7, 2013. Revised August 7, 2013. Accepted August 11, 2013. Advance Access publication October 30, 2013

Introduction

Accurate seizure localization is of vital importance both for clinical management and for understanding epileptic mechanisms. Seizure localization relies heavily on visual analysis of EEG in the delta-low gamma frequency bands (Rosenow and Lüders, 2001). However, this traditional method may result in a significant overestimation of the seizure core territory. In a previous study (Schevon *et al*., 2012), we described how multi-unit activity recorded during spontaneous human seizures allowed for a clear distinction to be made between territories that were fully recruited to the seizure, following passage of the ictal wavefront with its intense neuronal bursting participation, and territories that were on the periphery of this core recruited area, demonstrating low level, desynchronized firing. We use the terms 'ictal core' and 'ictal penumbra' for these two regions, respectively (shown schematically in Fig. 1B). Penumbral territories may subsequently be recruited into the ictal core territories, although this does not always happen.

Detailed studies of penumbral activity in simple slice models have revealed that neural firing is restrained by an 'inhibitory veto' effect, resulting from a strong feedforward inhibitory response to the powerful excitatory seizure core activity (Prince and Wilder, 1967; Trevelyan *et al*., 2006, 2007). Importantly from the perspective of EEG interpretation, low frequency signals temporally matched to those in recruited areas are very large in penumbral regions, ahead of the ictal wavefront (Trevelyan *et al*., 2006; Schevon *et al*., 2012). Thus, low frequency ictal rhythms cannot reliably distinguish the penumbra from the ictal core, which can confuse estimates of the site of origin and trajectory of spread. This may be a contributing factor to poor surgical outcomes in those neocortical syndromes where imaging fails to identify a

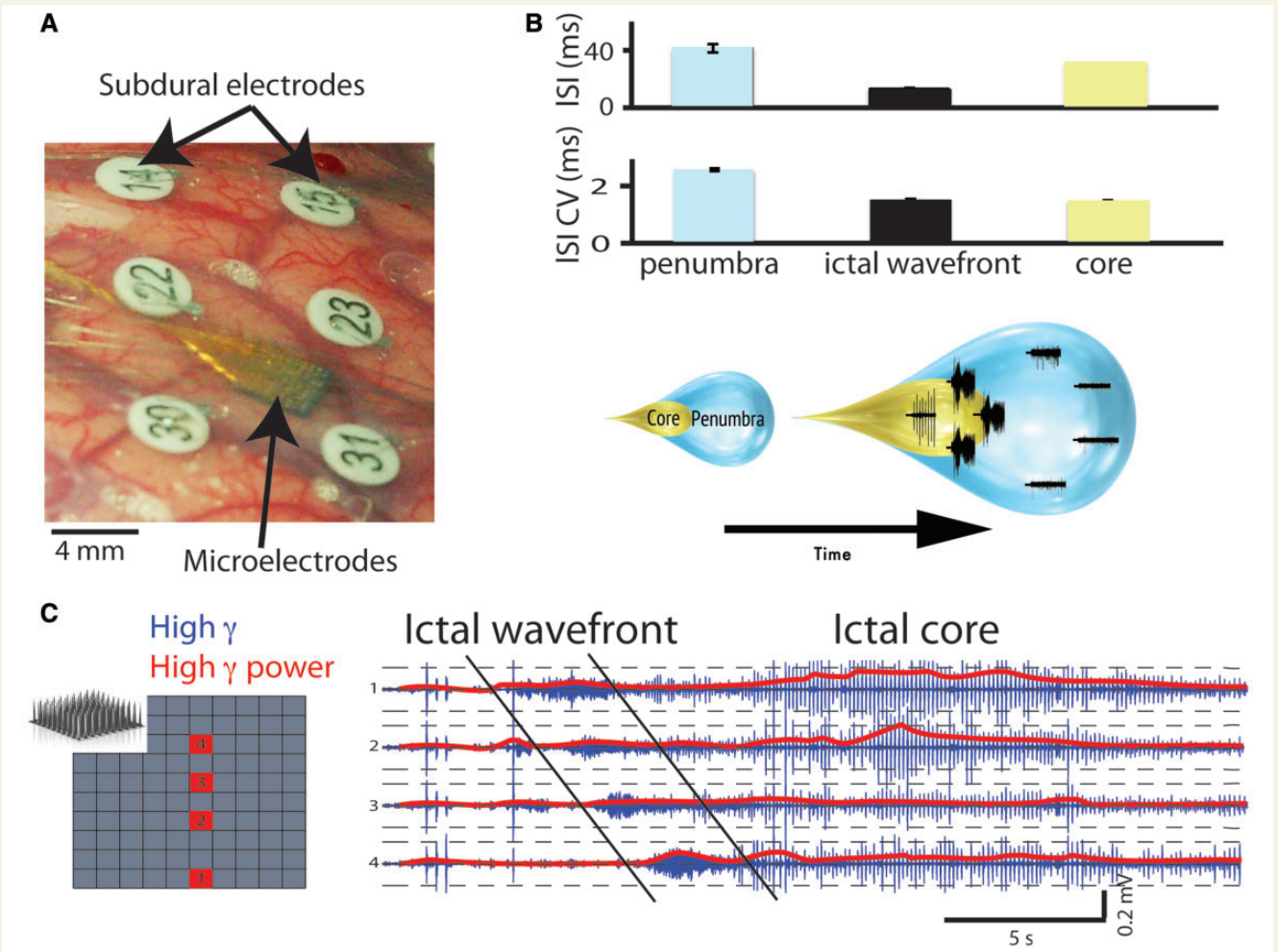

Figure 1 High gamma oscillations reflect neuronal firing patterns during a seizure. (**A**) Photograph of the recording arrangement in an epilepsy patient undergoing intracranial EEG monitoring. The subdural electrodes (numbered) surround the microelectrode array (arrow). (**B**) Schematic of the two distinct seizure territories, the core and penumbra. At any given moment, one can distinguish between the two territories on the basis of neuronal firing statistics such as inter-spike interval (ISI) and the coefficient of variation (CV) of the inter-spike interval. These territories expand as the seizure progresses. (**C**) Progression of the ictal wavefront across the microelectrode array (schematic, selected electrodes shown in red). High gamma filtered activity (blue) and high gamma power (red) are shown for each of the four electrodes. Note the periodic bursts in high gamma activity following passage of the ictal wavefront (diagonal black lines).

clear lesion (Rosenow and Lüders, 2001; Wetjen *et al*., 2009); only 30% of such patients are seizure-free at 5 years, compared with 60–80% of patients with mesial temporal lobe epilepsy or with syndromes associated with a well-defined structural lesion (Cohen-Gadol *et al*., 2006; Jeha *et al*., 2007).

The key questions remain then, what are the true localizing electrophysiological biomarkers, and what is the extent of the ictal core territory that they may reveal? High frequency oscillations (HFOs) have been proposed as an indicator of seizure-generating sites (Worrell *et al*., 2004; Jirsch, 2006; Engel *et al*., 2009; Jacobs *et al*., 2012), carrying information distinct from that provided by large, low-frequency discharges (Jacobs *et al*., 2008). We hypothesized that brain regions demonstrating low-frequency discharges during seizures, but lacking HFOs, correspond precisely with the ictal penumbra described in our previous study (Schevon *et al*., 2012). It is also important to establish context for the HFOs that are specific for the ictal core, as HFOs are likely to arise from multiple biophysical mechanisms (for review, see Menendez de la Prida and Trevelyan, 2011). In contrast to interictal HFOs, ictal HFOs are more likely to have specific localizing value. Sites with high rates of ictal HFOs correspond well with the clinically-determined seizure onset zone, which encompasses both core and penumbral territories (Ochi *et al*., 2007; David *et al*., 2011; Modur *et al*., 2011; Fujiwara *et al*., 2012; Park *et al*., 2012). It is noteworthy that one study limiting resections to brain areas demonstrating sustained ictal HFO activity reported comparable success rates to standard treatments, for which resections are typically far larger (Modur *et al*., 2011). The development of extended microelectrode arrays now allows for a more rigorous test of the HFO-biomarker hypothesis.

We propose that repetitive, delayed-onset, high frequency oscillations (80–150 Hz) recorded from standard subdural electrodes during seizures correspond precisely to core regions of epileptic activity as defined by multi-unit recordings. Specifically, we hypothesize that the burst firing that occurs during a paroxysmal depolarizing shift, synchronized across several millimetres of neocortex, results in a transient increase in high gamma amplitude. It is these transient amplitude increases that are detected from clinical electrodes recording at the cortical surface as high frequency oscillations. To test our hypothesis, we used our existing seizure recordings from patients undergoing long term intracranial EEG monitoring, who also had microelectrode arrays implanted in the epileptic cortex. This allowed us to discern the core and penumbral areas in the entire area sampled by subdural electrodes, and to validate our findings of high frequency activity recorded from subdural electrodes close to the microelectrode array. Thus, we can map the evolution and spread of the seizure core, and contrast it to the low-frequency, large amplitude EEG activity that has traditionally been used to define seizure-generating areas.

Materials and methods

Study participants consisted of adults with pharmacoresistant focal epilepsy who underwent chronic invasive EEG studies to help identify the epileptogenic zone for subsequent removal. A 96 channel, 4 mm × 4 mm microelectrode array was implanted along with subdural electrodes with the goal of recording from seizure onset sites. The study was approved by the Institutional Review Board of the Columbia University Medical Centre, and informed consent was obtained by each patient before implantation. Refer to the Supplementary material and Schevon *et al*. (2012) for details of study enrolment and surgical procedures.

Signals from the microelectrode array were acquired continuously at 30 kHz per channel (0.3 Hz–7.5 kHz bandpass, 16-bit precision, range ± 8 mV). The reference was either subdural or epidural, chosen dynamically based on recording quality. Subdural EEG signals were acquired using a standard clinical video EEG system (XLTek, Natus Medical Inc) at 500–2000 Hz per channel (0.5 Hz high pass, low pass set to 0.25 times the sampling rate, 24-bit precision). The two data sets were aligned using a pulse-coded signal delivered simultaneously to digital input ports of both recording systems.

The first three seizures (if available) from each patient were selected for detailed analysis, to avoid biasing the data set from the patients from whom many seizures were recorded. Channels and time periods with excessive artefact or low signal-to-noise ratio were excluded. Raw microelectrode signals were bandpass filtered (symmetric 1000th order finite impulse response) into high gamma (80–150 Hz) and multi-unit activity (300 Hz–3 kHz) data streams. Because some subdural data were sampled at 500 Hz, 150 Hz was selected as a practical upper limit for the high gamma band; further, little useful subdural signal was detected at frequencies > 150 Hz. Action potentials were detected from multi-unit activity by identifying negative peaks with amplitudes > 2.5–4 SD (standard deviations) below the mean (Busse *et al*., 2009). We did not attempt to isolate single units, as the destructive interference resulting from large numbers of simultaneously discharging neurons in the seizure core within the listening sphere of the microelectrode would confound any attempt to classify and sort action potential waveforms.

The ictal wavefront was identified by its distinctive pattern of sudden onset of continuous firing lasting 1–2 s, followed by a transition to rhythmic burst firing alternating with periods of neuronal inactivity (Goldensohn and Purpura, 1963). The ictal wavefront was then used to divide seizure epochs into penumbral (after seizure onset but before the ictal wavefront, or the entire seizure duration if no wavefront was detected) and core territories (region of rhythmic burst firing following passage of the ictal wavefront). See Supplementary material for details of multi-unit activity analysis.

Cross frequency coupling was measured using modulation index and phase-locking value, both based on instantaneous phase and amplitude calculated from the Hilbert transform. Modulation index is defined from two signals as

$$MI_{raw} = \left| \frac{1}{N} \sum_{n=1}^{N} a_1[n] \exp(i^* f_2[n]) \right| \quad (1)$$

where a_1 is the instantaneous amplitude of the first signal, and f_2 is the instantaneous phase of the second signal. The raw values are then normalized using a surrogate data approach, as described in Canolty *et al*. (2006). Modulation index was calculated across the entire duration of the seizure in 0.5 Hz bins between 2–20 Hz for f_2 and in 5 Hz bins between 2–202 Hz for a_1.

Phase-locking value (PLV; Penny *et al*., 2008), a measure of phase correlation that varies in the [0 1] interval, is defined as

$$PLV = \left| \frac{1}{N} \sum_{n=1}^{N} \exp(i(\phi_{4-30Hz}[n] - \phi_{a(80-150Hz)}[n])) \right| \quad (2)$$

where $\phi_{a(80-150Hz)}$ is calculated from a second Hilbert transform applied to the instantaneous amplitude of the high gamma filtered

signal. Phase-locking value was calculated in sliding windows of 3 s, advanced in 333 ms increments.

The phase-locked high gamma (PLHG) calculation,

$$PLHG = \left| \frac{1}{N} \sum_{n=1}^{N} a_{norm(80-150Hz)} \exp(i(\phi_{4-30Hz}[n] - \phi_{a(80-150Hz)}[n])) \right| \quad (3)$$

weights instantaneous high gamma (80–150 Hz) amplitude, normalized to the pre-ictal baseline, by the simultaneous phase-locking value with low frequency (4–30 Hz) phase. PLHG time series were also calculated using the sliding window method as described above. This measure produces similar results to measures based on HFO rates, but is more efficient to implement and automatically discounts spurious or artefactual HFOs (e.g. from cardiac artefact). Ictal core recruitment was defined based on PLHG values increasing to 2.5 SD over the mean. In Patients A and B values were calculated only over the initial 25 s of the seizure due to skew in the sample introduced by large areas of late recruitment.

Line length (Esteller *et al*., 2001) was calculated from filtered EEG (2–25 Hz, 500th order symmetric finite impulse response filter) and normalized to a 30 s pre-ictal baseline. Channel recruitment was defined based on line length values increasing to 2.5 SD over the mean (Schindler *et al*., 2007). Normalized Levenshtein distance, a measure of the minimum distance between two sequences, was used to calculate the stereotypy of seizure spread using both PLHG and line length criteria (Schauerte and Fink, 2010).

Results

Ten spontaneous seizures, lasting between 14–102 s, were recorded from four patients with neocortical epilepsy using both the 96 channel microelectrode array and 43–84 subdural electrodes arranged in grids and strips overlying the array (Fig. 1A). In four seizures (two patients), the microelectrode arrays recorded periods of both full seizure activity and penumbral activity, whereas the remaining six seizures (two patients) included only penumbral activity patterns. In total there were 203 high-quality microelectrode recordings of full seizure activity, including both penumbral and ictal core activity, 220 of penumbral activity alone, and 672 subdural electrode recordings.

Multi-unit firing as the basis of increased high gamma amplitude

The ictal core and penumbra (Schevon *et al*., 2012) were clearly distinguished by their signature neuronal firing patterns, and sharply demarcated spatially by the narrow ictal wavefront at the leading edge of the seizure core (Fig. 1B and C and Supplementary Table 1). In two patients (Patients B and A), passage of the ictal wavefront with intense, continuous firing was noted in all microelectrode channels, followed by repetitive synchronized burst firing time-locked to the low-frequency (<25 Hz) ictal discharges. In the remaining two patients (Patients D and C), firing remained heterogeneous and poorly phase-locked to the low-frequency ictal discharge throughout (Schevon *et al*., 2012), with no evidence of an ictal wavefront. Thus, there were clear qualitative differences between these recordings: the recordings from Patients B and A were from areas that were recruited into the ictal core, whereas the recordings from Patients D and C were penumbral.

We next sought to establish whether instantaneous high gamma amplitude is a useful index of multi-unit firing. We observed this first by visual inspection of microelectrode-recorded high gamma (Fig. 2A and Supplementary Fig. 3E), which shows activity patterns similar to those described above in multi-unit firing (Fig. 1C). We then developed additional lines of evidence to establish a precise temporal correlation using the microelectrode recordings. Spike (action potential)-triggered averaging of unfiltered field potential signals before and during the seizure (Fig. 2B) revealed that units were time-locked to the trough of oscillations in the high gamma range (Supplementary Fig. 1 and Supplementary Table 1). Examination of Spearman correlation between multi-unit firing rates and field potential spectral power for the pre-ictal and ictal epochs revealed a monotonic relationship between the frequency of the oscillation, with high gamma as the lowest frequency band with significant correlation (Fig. 1C, grey band). The lowest frequency for which field potential power was significantly correlated with multi-unit firing rate during the seizure averaged 62.1 ± 7.4 Hz, with 75.8 ± 15.2% of microelectrodes meeting statistical significance (Fig. 1C, black arrow). Linear regression slope of ictal high gamma amplitude with respect to multi-unit firing rate was greatly increased in the ictal epoch compared with both the pre-ictal epoch (two-tailed paired *t*-test, $n = 423$ microelectrodes, $P < 0.001$, Supplementary Fig. 2). No difference in regression slope was evident across patients during the pre-ictal epoch (Supplementary Fig. 2B, two tailed unpaired *t*-test, $n = 423$ microelectrodes, $P = 0.3$).

We further hypothesized that subdural detection of high gamma activity depends not only on firing rate, but also on the degree to which multi-unit firing is synchronized across the electrode's recording area. In the ictal core, multi-unit 'hyper-synchronization' of the firing bursts was prominent across the entire territory sampled by the multi-electrode array (Fig. 3A and D) (Schevon *et al*., 2012). Multi-unit cross-correlation in the ictal core was significantly increased from the pre-ictal period (Fig. 3C and D), as was the number of channel pairs exhibiting a significant correlation as tested with a bootstrap procedure ($P < 0.05$, Supplementary material, two-tailed paired *t*-test, $n = 4$ seizures, $P < 0.01$). Subdural seizure recordings from electrodes overlying or adjacent to the microelectrode array demonstrated significant increases in high gamma activity after the ictal wavefront had passed across the microelectrode territory, ~8 s after seizure onset for Patient A, and 14 or more seconds after seizure onset for Patient B (two-tailed unpaired *t*-test, $n = 4$ seizures, $P < 0.001$), but not during ictal wavefront passage (Fig. 3A). Ictal subdural high gamma amplitude also increased in penumbral recordings, but the increase was significantly smaller than that in the ictal core (two-tailed unpaired *t*-test, $n = 10$ seizures, $P < 0.001$). In the penumbra, even though multi-unit firing rate increases up to 5-fold (Schevon *et al*., 2012), synchronization of multi-unit activity was not appreciably increased compared to the pre-ictal period (Fig. 3E–G, two-tailed paired *t*-test, $n = 6$ seizures, $P = 0.3$), reflecting the heterogeneous multi-unit firing pattern.

The strong transient increases in the high gamma band limited to ictal core territories, following passage of the ictal wavefront, result in ictal HFO detections in standard subdural recordings (Figs 2D and 3A and D). We noted, however, that HFOs

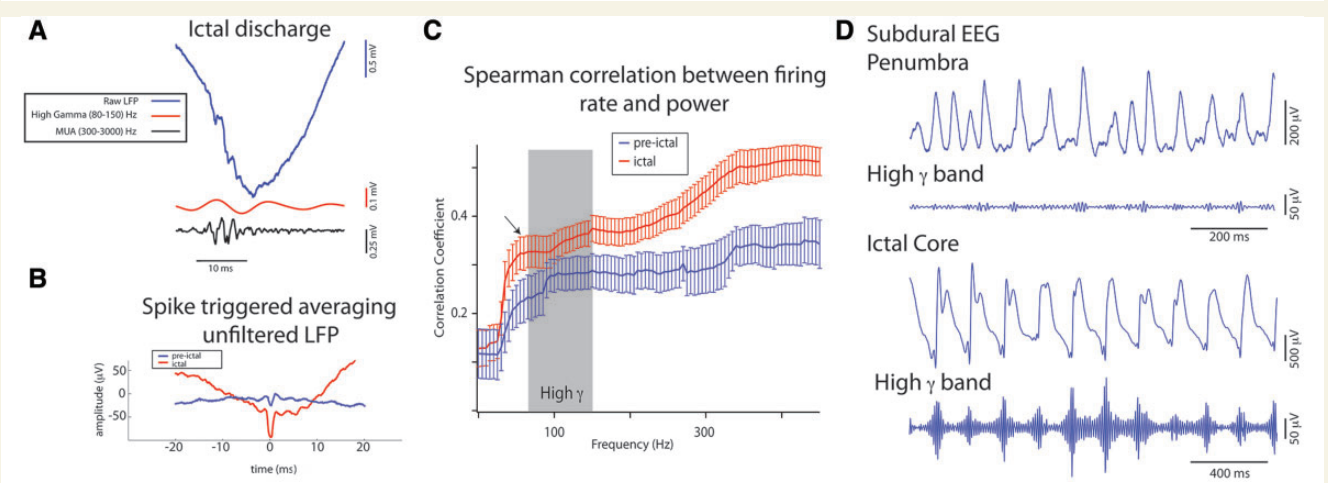

Figure 2 Ictal high gamma activity is tightly associated with unit activity and can be detected with subdural electrodes. (**A**) High gamma oscillations (red) and multi-unit activity (MUA, black) coincide during an ictal spike recorded by a microelectrode before filtering (blue). (**B**) Spike triggered averaging of the unfiltered local field potential (LFP) recorded by a microelectrode in the ictal core during pre-ictal (blue, $n = 109$ spikes) and ictal (red, $n = 204$ spikes) epochs. (**C**) Mean absolute Spearman rank correlation (r) of the linear fit between multi-unit firing rate and power (1–500 Hz) calculated in 5 Hz bins during the 10 s pre-ictal interval (blue, $n = 10$), and during the seizure (red, $n = 10$). The correlation during the ictal epoch reaches statistical significance at 62 Hz (arrow), just below the lower limit of the high gamma frequency band (shaded). (Spearman rank correlation, $n = 101$ spectral bins, 80–200 temporal bins, 423 microelectrodes, $P < 0.001$, Bonferroni corrected). The ictal correlation coefficients were increased compared with the pre-ictal baseline [one-way ANOVA, $F(19,100) = 127.3$, $P < 0.001$]. (**D**) Unfiltered and high gamma band pass filtered ictal recordings from the subdural electrode overlying the microelectrode array from two patients. Increased high gamma amplitude is visible at the negative peak of the low-frequency rhythm in the broadband signal recorded in the ictal core (Patient B) but not in the penumbral recording (Patient C).

superimposed on high-amplitude ictal discharges can be difficult to discern before filtering (Urrestarazu *et al.*, 2007). In these cases, they can be more easily distinguished from the spread of energy arising from sharp transients by their appearance on time-frequency spectrograms (Bénar *et al.*, 2010). We noted that the presence of spectrogram 'islands', as well as increased power in the 80–150 Hz band coinciding with the low-frequency discharge peaks, successfully distinguished sites with synchronized multi-unit firing from sites with heterogeneous firing (Supplementary Figs 3 and 4). This observation further supports focusing subsequent analysis on the 80–150 Hz band, chosen in recognition of the limited sampling of our clinical recordings (500 Hz) and to maintain consistency with the previous literature (Staba *et al.*, 2002; Grenier *et al.*, 2003; Jacobs *et al.*, 2008).

Phase-locked high gamma amplitude differentiates core from penumbra

We observed that in the ictal core, the peaks of ictal discharges coincided with both the multi-unit firing burst and the transient increases in high gamma amplitude that are the defining features of delayed-onset ictal HFOs (Fig. 3D and Supplementary Fig. 3). Conversely, high gamma amplitude is relatively low at other phases of the low-frequency (1–25 Hz) ictal discharges. Thus, multi-unit activity, instantaneous high gamma amplitude, and low-frequency ictal discharge phase are tightly coupled (Fig. 4A and B). In contrast, this hierarchical arrangement was not found in penumbral recordings (Fig. 4C). Specifically, multi-unit firing was not significantly related to the phase of the low frequency ictal rhythm (Schevon *et al.*, 2012), nor was it synchronized with the peak amplitude of the high gamma oscillations (Fig. 3H). Coupling of high gamma amplitude to low frequency (2–25 Hz) phase in both the microelectrode and the overlying or adjacent subdural recordings (Fig. 5A) was measured using phase-locking value and modulation index. There was a high correspondence between the two recording modalities (Fig. 5B, phase-locking value, $R^2 = 0.8$, $F = 23.8$, $P < 0.01$, $n = 10$). The coupling measures were consistently higher in subdural recordings of the ictal core, compared to the penumbra (Fig. 5B and D; phase-locking value; $n = 4$ ictal and six penumbral recordings, two-tailed unpaired t-test, $P < 0.01$), and correlated well with measured multi-unit cross-correlation (Fig. 5C and D; $n = 10$, $R^2 = 0.4$, $F = 5.8$, $P < 0.05$). This was also true when we compared dynamic measures of phase-locking value and multi-unit cross correlation (Fig. 5C and Supplementary Table 2).

As subdural high gamma amplitude and cross frequency coupling both tracked local neural burst firing and synchronization in the underlying cortex, we developed the PLHG metric to capture the transient increases in high gamma amplitude and their low-frequency context that marks ictal core recruitment (Fig. 6). PLHG values reached the detection threshold in all electrodes adjacent to or overlying the microelectrode array in the four seizures demonstrating ictal wavefront and core activity in the microelectrode recordings. In all six seizures in which the microelectrode array recorded only penumbral activity, the overlying or adjacent subdural electrode showed PLHG that was significantly smaller than in other adjacent grid electrodes (two-tailed paired t-test, $n = 6$ seizures, $P = 0.02$). In Patient C, the PLHG measured from the

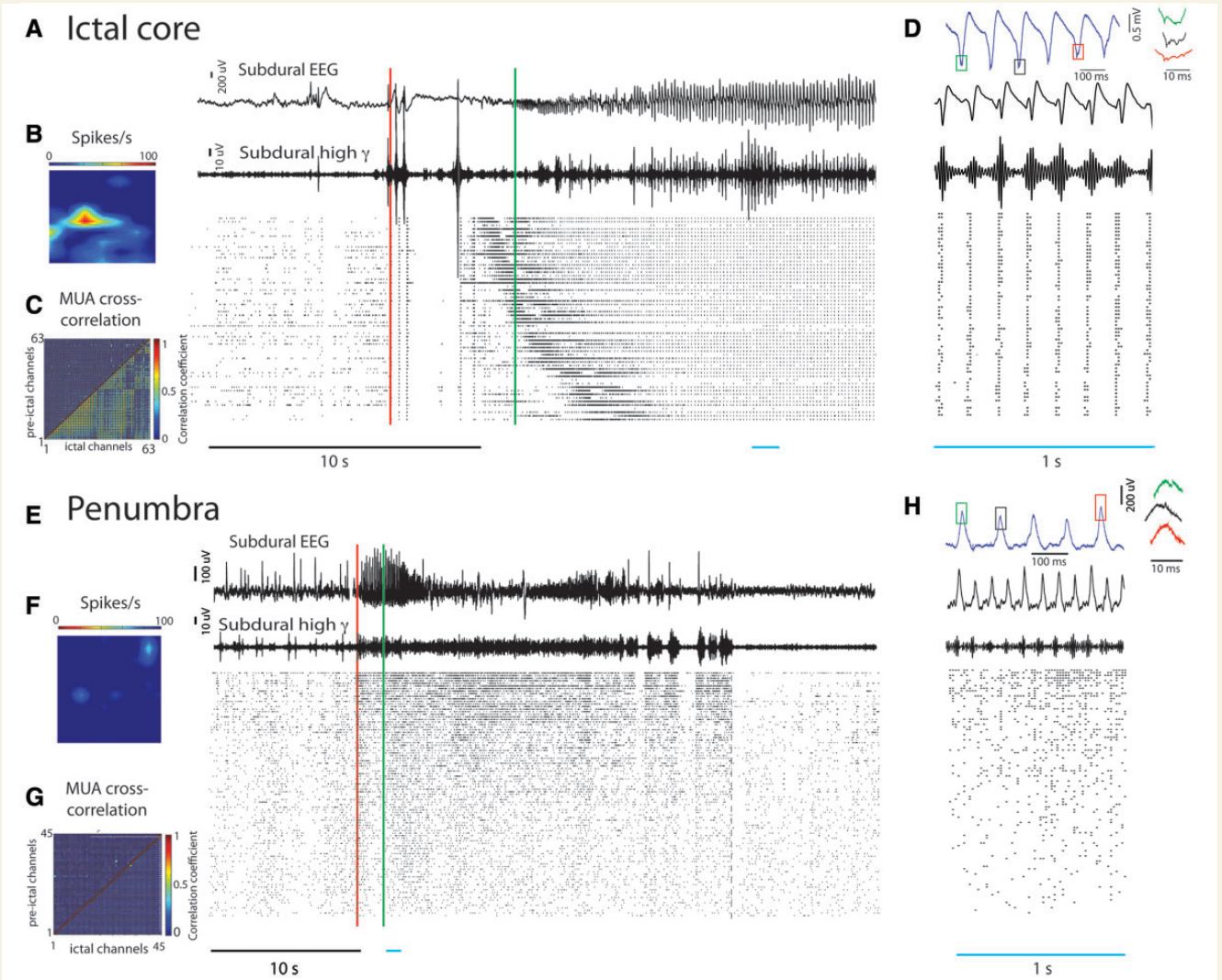

Figure 3 Hypersynchronization is evident in the ictal core but not the penumbra. (**A–D**) Analysis of ictal core activity. (**A**) EEG recorded from a subdural electrode adjacent to the microelectrode array in Patient A. Note the high gamma bursts developing late in the seizure (onset indicated by red line). (**B**) Raster plot of detected action potentials, sorted in order of recruitment and time-locked to the EEG. Spatial map of multi-unit firing at the time indicated by the green vertical line demonstrating the propagating ictal wavefront (*left*). (**C**) Multi-unit cross correlation coefficient measured during the 30 s pre-ictal interval (upper diagonal) and during the seizure (lower diagonal). (**D**) *Top*: Ictal microelectrode recording illustrating high frequency oscillations (*right*) at the negative peak of the low-frequency rhythm (coloured squares). *Bottom*: Enlarged timescale of the period indicated by the blue bar. Note the extreme hypersynchrony across all microelectrode channels, with high gamma amplitude peaks aligning with negative peaks of the low-frequency ictal rhythm. (**E–H**) Similar presentation of penumbral activity. (**E**) EEG recorded from subdural electrode partially overlying the microelectrode array in Patient C. The corresponding high gamma band pass filtered signal does not demonstrate the bursting present in **A** and **D**. Corresponding raster plot showing the absence of an ictal wavefront and ictal core stage. (**F**) Spatial map of multi-unit firing at time indicated by the green arrow fails to identify a propagating wavefront. (**G**) Multi-unit cross correlation coefficients as in (**C**). (**H**) *Top*: Closer examination of the positive peaks, to which small high gamma transients were aligned, reveals no oscillatory activity. Interval indicated by blue bar at higher temporal resolution demonstrating minimal amplitude modulation of the high gamma band relative to the phase of the ictal rhythm, and no phase-locking of units. MUA = multi-unit activity.

electrode overlying the microelectrode array never reached threshold (Fig. 6B). In Patient D, recordings from the two electrodes superior to the microelectrode implant site met PLHG threshold criteria, but that was not the case for the two electrodes inferior to the implant site, including the nearest adjacent electrode. Such sharp spatial gradients in PLHG values were not uncommon. An example of microelectrode-recorded penumbral activity within 1 cm of strong HFO activity and increased PLHG values is shown in Fig. 7 (left panels). The overlying subdural electrode showed low amplitude, minimally fluctuating signal in the high gamma band, but there was greatly increased power and PLHG in the adjacent electrode in one direction, although notably not in other directions. An example of microelectrode-recorded ictal core activity is shown (Fig. 7, right panels), demonstrating large

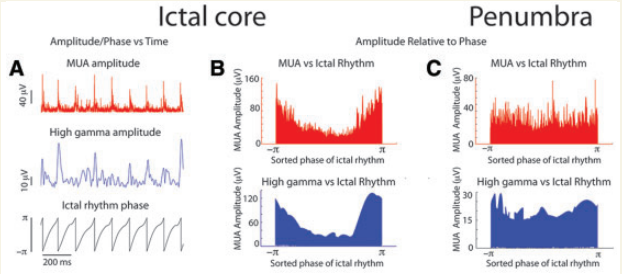

Figure 4 Hierarchical cross frequency coupling between the ictal rhythm, high gamma, and multi-unit activity is evident in the ictal core, but not in the penumbra. (**A**) One second intervals of the instantaneous phase of the ictal rhythm from a microelectrode recording of ictal core activity (*bottom*). Corresponding instantaneous high gamma (*middle*) and multi-unit (*top*) amplitude during this epoch. (**B**) For the entire duration of the microelectrode recording of the ictal core the instantaneous phase was sorted (*bottom*) and the permutation vector was applied to the amplitude of the high gamma band (*middle*) and the amplitude of the multi-unit activity (*top*). (**C**) This same analysis was applied to the entire duration of a microelectrode recording from the penumbra but no clear relationship to low frequency phase was evident.

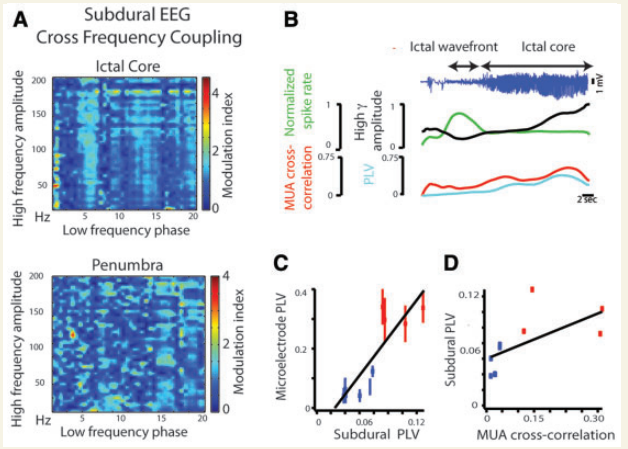

Figure 5 Cross frequency coupling in subdural EEG seizure recordings. (**A**) Cross frequency coupling as quantified by the modulation index (see 'Materials and methods' section). The top plot shows a seizure recording from a subdural electrode overlying the ictal core, as defined by multi-unit firing from the microelectrode array. Note that the modulation is maximal between the phase of the ictal rhythm (prominent vertical band at ~5–7 Hz and harmonics) and the high gamma band (~90–180 Hz). In contrast, cross-frequency coupling is not prominent in a recording from the penumbra in another patient. The ictal rhythm in this case is in the 10–12 Hz range. (**B**) Linear correlation of subdural EEG and microelectrode local field potential phase-locking value (PLV), another measure of cross frequency coupling between high gamma (80–150 Hz) and lower frequencies (4–30 Hz), for seizures recorded from the ictal core (red, $n = 4$), and the penumbra (blue, $n = 6$), showing clear distinction between the two regions. (**C**) Subdural high gamma amplitude (black) departs significantly from the normalized multi-unit firing rate (green) during a seizure (blue, *top*), while subdural phase-locking value (cyan) closely tracks multi-unit cross-correlation (red). (**D**) Linear correlation between subdural phase-locking value and multi-unit activity correlation coefficient for seizures recorded from the ictal core (red, $n = 4$), and the penumbra (blue, $n = 6$).

amplitude, high gamma signal in the overlying subdural electrode, but greatly reduced high gamma signal in an adjacent electrode, 1 cm distant.

We also compared the timing of PLHG recruitment in the electrodes adjacent to or overlying the microelectrode array, for the four seizures demonstrating ictal core activity. For Patient A, the ictal wavefront passage was complete at 5.6 s after seizure onset, and the PLHG measure reached threshold in the nearest adjacent electrode at 6.4 s. For Patient B's three seizures, the ictal wavefront passage was completed at 18.9, 21.0, and 23.4 s, and PLHG threshold was reached in the overlying electrode at 22.3, 28.7, and 26.2 s, respectively. In all cases, the PLHG measure reached the detection threshold after the ictal wavefront had completed its passage through the microelectrode sampled area, with an average lag of 3.4 s (Figs 3A and 8A–C). Thus, in all 10 seizures, a simple metric designed to detect sustained discharge-associated HFOs gave an accurate indication of the seizure progression as revealed by the microelectrode array.

Mapping seizure spread globally using subdural recordings

In all cases, the PLHG measure revealed sharp divisions between the presumptive core and penumbra territories, and easily defined spread of the core ictal activity. Ictal core origination and spread are depicted in videos of a single seizure from each patient (Supplementary Videos 1–4), with key time points shown in Fig. 8. The presumptive ictal core eventually surrounded the microelectrode array implant site during all four seizures in which core seizure activity was detected by the microelectrodes (Fig. 8A–C and Supplementary Videos 1 and 2). In the remaining six seizures in which only penumbral activity was seen in the microelectrode recordings, the presumptive ictal core skirted the implant site although it came within 1 cm of the site in all cases (Fig. 8D and E and Supplementary Videos 3 and 4). Further, the direction of ictal wavefront progression in the microelectrode array matched the direction of expansion of the subdurally detected ictal core in the vicinity of the microelectrode array (Fig. 8B).

To compare this view of seizure core areas to the results of standard EEG interpretation, we quantified the seizure territory that would normally be visualized in the low-frequency (1–25 Hz) EEG band using an established line length measure (Esteller *et al.*, 2001; Schindler *et al.*, 2007). Seizure spread was measured at 6.2 ± 0.9 channels/s, significantly faster than the ictal core recruitment rate of 0.5 ± 0.3 channels/s (Fig. 8C, E and F, two-tailed paired *t*-test, $n = 10$ seizures, $P < 0.01$). Variability of ictal core recruitment within and across patients was lower than the variability of seizure spread under line length criteria (Fig. 8G,

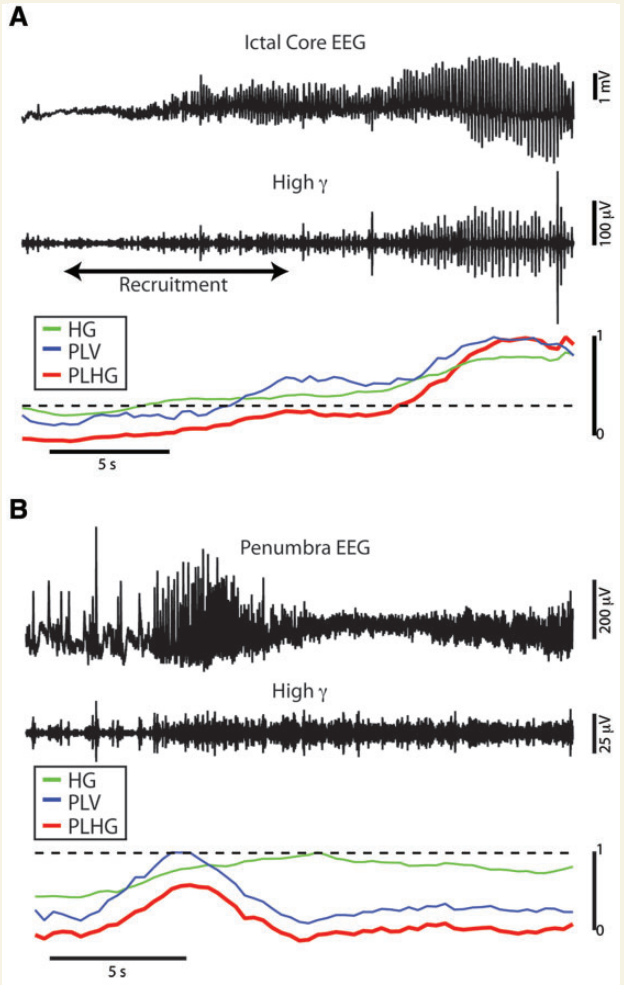

Figure 6 The phase-locked high gamma metric as a measure of high gamma amplitude weighted by low frequency coupling. (**A**) Seizure recorded from a subdural electrode in the ictal core adjacent to the microelectrode array, showing wideband EEG (*top*) and 80–150 Hz filtered signal (*middle*). The *bottom* plot shows corresponding normalized traces of high gamma amplitude (HG, green), phase-locking value between the ictal rhythm and the high gamma band (PLV, blue), and phase-locked high gamma amplitude (PLHG, red). The dotted line indicates a Z-scored PLHG value of 2.5. Note that the PLHG measure accurately tracks high gamma amplitude coupled to the phase of the ictal rhythm, and that high gamma amplitude increases can be seen before recruitment as indicated by the microelectrode recording (black arrows). (**B**) Similar recording from a subdural electrode overlying the microelectrode array, at a site showing only penumbral activity.

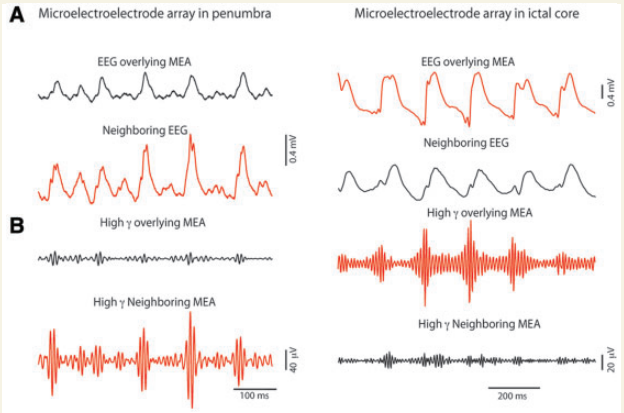

Figure 7 Sharp spatial gradients in low-frequency coupled high gamma amplitude, but not in low frequency EEG. (**A**) Wideband EEG recorded from pairs of subdural electrodes (1 cm separation), with one electrode in each pair overlying the microelectrode array (MEA), in two patients, one with the microelectrode array situated in penumbra (*left*), and one with the array located in a recruited area (*right*). In each case, penumbral (definite or presumed) sites are indicated by black traces, and ictal core by red traces. Signal from the electrodes overlying the microelectrode array is slightly attenuated, due to partial blockage of the recording area. Otherwise, the tracings are similar. (**B**) High gamma bandpass filtered signal from the same pairs of electrodes during the time epochs indicated by the black bars, demonstrating amplitude modulated high gamma in the ictal core but not in the adjacent penumbra.

normalized Levenshtein distance, two-tailed paired *t*-test, $n = 9$, $P < 0.01$).

Given the ability to divide the seizure territory into core and penumbra areas, the extent of the ictal core is of immediate clinical and practical importance. The number of channels included in the subdurally detected ictal core, including late seizure spread but exempting secondary generalization, averaged 10.9 ± 1.3 across all 10 seizures. In contrast, the total number of channels recruited into the seizure using line length criteria was 62.5 ± 6.0, a significantly greater extent (two-tailed paired *t*-test, $n = 10$ seizures, $P < 0.01$, Fig. 8). Thus, the ictal core as detected by applying the PLHG to subdural recordings was found to comprise an average of 17% of the cortical territory exhibiting seizure activity on the basis of the line length measure, judging from maximal seizure spread either to seizure offset, or to the point of secondary generalization (Patient A). This difference is even more marked in the early seizure stages (Fig. 8).

Discussion

Considerable evidence has been amassed associating bursts of high frequency brain rhythms with epileptic pathology, but the exact relationship and underlying mechanisms have remained controversial. Using spatially extensive subdural recordings together with dense microelectrode sampling of a small area within the clinically identified seizure onset zone, we have provided key evidence that the core areas recruited into spontaneous human seizures are marked in clinical subdural recordings by the delayed appearance of HFOs phase-locked to the low-frequency ictal discharges. These HFOs correspond to intense, synchronized multiunit burst firing in the underlying cortex. The delayed appearance is because of the slow propagation of the ictal wavefront, which cannot be reliably detected by large subdural electrodes.

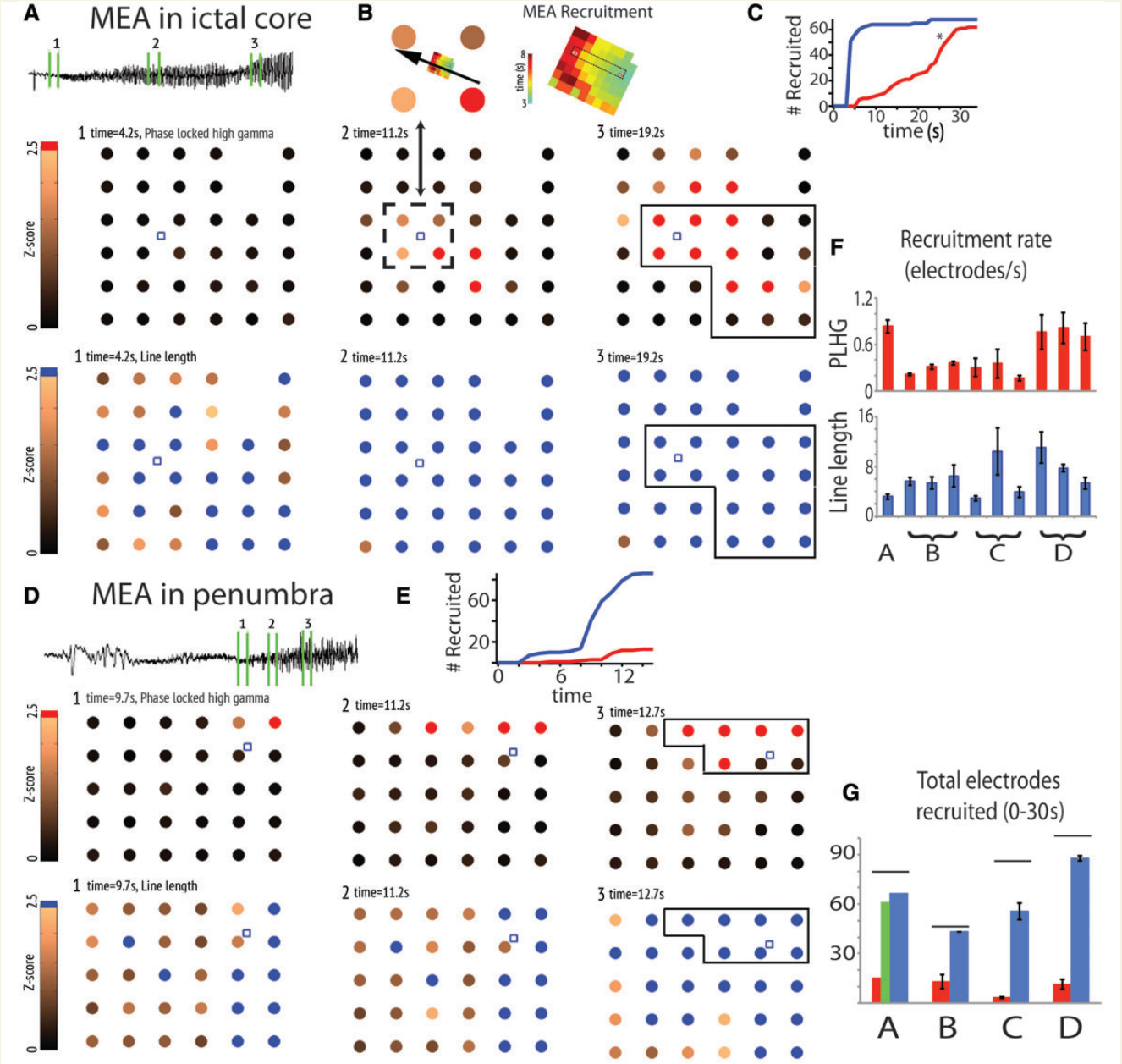

Figure 8 Mapping seizure activity using the phase-locked high gamma metric. Subdural electrode grids in Patient A (**A–C**) and Patient D (**D–E**), with the location of the microelectrode array (MEA) indicated by the small blue box and the seizure onset zone outlined in black. The copper colour scale indicates the z-scored PLHG (**A** and **D**, *above*), and z-scored line length (**A** and **D**, *below*) relative to the pre-ictal baseline, capped at the threshold value of 2.5 as indicated by the colours red (PLHG) and blue (line length). (**A** and **D**) PLHG (*top*) and line length (*bottom*) values at three time intervals during the seizure denoted by the green numbered bars superimposed on the corresponding EEG. Note that the spread of PLHG was spatially contiguous, with a clear area of origin and path of propagation. The site of the microelectrode array was incorporated into the PLHG-defined core region in Patient A, but not in Patient D, matching the site classification afforded by the multi-unit recordings. (**B**) The direction of spread was also consistent with the direction of ictal wavefront propagation recorded from Patient A, judged from MUA firing rate peak latencies and correlating array placement using the intraoperative photo in Fig. 1A. (**C** and **E**) Plot of the total number of subdural electrodes recruited into the seizure by each measure as a function of time. The asterisk indicates approximate time of secondary generalization, based on clinical semiology. (**F**) Summary bar graph of the recruitment rate by PLHG (red) and line length (blue) for the 10 seizures recorded from the four patients. Error bars indicate 95% confidence intervals. (**G**) Bar plot of the percentage of total electrodes that were recruited into the ictal core or penumbra for each of the four patients. For Patient A, the red bar indicates PLHG recruitment up to the point of secondary generalization, and the green bar indicates total PLHG recruitment.

Conversely, we show that the surrounding ictal penumbra, marked by heterogeneous, low-level multi-unit firing, lacks the transient high gamma amplitude increases that characterize HFOs. Because the low frequency discharges in the ictal core and penumbra appear similar (Schevon *et al*., 2012), this observation suggests a clinically useful method of differentiating the two regions. A practical measure incorporating cross-frequency coupling of high gamma amplitude with the phase of low-frequency ictal discharges was used to map the extent and progression of the seizure core in the clinical recordings. We demonstrated that these maps are consistent with the 'gold-standard' information provided by the microelectrode recordings, and also with the expected range for seizure propagation speed. Most strikingly, we found that the seizure core is far smaller than the areas defined using traditional EEG interpretation.

Our findings not only serve to confirm the clinical impression of HFOs as a potentially useful clinical biomarker of seizure-generating areas, but they also clarify the context for interpreting HFOs in clinical intracranial EEG recordings. Historically, HFOs have been defined and classified based solely on their signal characteristics, with no clear consensus regarding which features are specific for seizure-generating sites (Engel *et al*., 2009). It is important therefore to relate HFO patterns to neuronal firing patterns recorded over an extended cortical territory, as these provide the most accurate seizure localizing information.

Generators of subdurally recorded ictal high frequency oscillations

It is clear that multi-unit firing in the ictal core is associated with increased high gamma amplitude for both microelectrode and subdural recordings. Fast ripples (>200 Hz) recorded by microelectrodes *in vitro* have been ascribed to pyramidal cell firing (Bragin *et al*., 2002; Dzhala and Staley, 2004; Foffani *et al*., 2007), but the source of 80–150 Hz activity recorded from subdural electrodes has not yet been fully characterized. It is likely that some high frequency oscillations may be attributed to temporal alignment of pyramidal cell firing by synchronized interneuron activity (Ylinen *et al*., 1995; Trevelyan, 2009), reflecting strong inhibitory currents that are likely to be particularly intense in penumbral territory (Trevelyan *et al*., 2006, 2007). It is therefore possible that only some types of pathological HFOs are specific for seizure-generating regions.

It should be noted that the delayed-onset, ictal HFOs that are the focus of our study should be considered as distinct from the early-onset HFO activity and/or increased high gamma power that has long been reported as a possible marker of the seizure-onset zone (Fisher *et al*., 1992; Alarcon, 1995; Worrell *et al*., 2004; Jirsch, 2006). Recently, it has been proposed that such early activity may not be as reliable a marker as delayed-onset HFOs (Modur *et al*., 2011). Indeed, such transient, early HFO activity was noted in one of our patient recordings (Patient B), but it did not predict the appearance of delayed onset, persistent HFOs. Further research will be necessary to establish the mechanisms and descriptive characteristics of these different classes of high frequency rhythms.

Instead, high gamma activity in seizure core territories is most likely generated from the intense firing that accompanies paroxysmal depolarizing shifts. Spectral overlap of synchronized action potentials, phase-locked to the trough of the high gamma rhythm, has been noted in previous studies of non-epileptic animal and human recordings (Grenier *et al*., 2003; Le Van Quyen *et al*., 2008; Ray and Maunsell, 2011; Scheffer-Teixeira *et al*., 2013). This property was also evident in our recordings of spontaneous human seizures (Fig. 2B, Supplementary Fig. 1 and Supplementary Table 1). In addition, detailed biophysical modelling suggests that the periodicity of action potentials (Supplementary Table 1) during ictal discharges may contribute substantial power to the high gamma band (Schomburg *et al*., 2012).

High gamma activity recorded from subdural electrodes is not precisely equivalent to microelectrode-recorded high gamma, because spatial averaging, distance from deeper cortical layers and low impedance impairs detection of potentials with small fields. For high gamma activity to appear in subdural EEG signals, multi-unit firing must be synchronized in the recording area (Ray *et al*., 2008). If the increase in high gamma amplitude recorded from subdural electrodes simply reflected the change in firing rate, then it would peak at the ictal wavefront itself. This, however, was not the case: the persistent increase in subdural high gamma amplitude was reliably detected only later in the seizure, after the passage of the ictal wavefront, as overall multi-unit firing concentrated into brief bursts and became more synchronized across an extended cortical territory (Figs 3A and 5C). The delayed appearance of sustained, bursting ictal high gamma activity in the subdural recording can then be attributed to the slow (<1 mm/s) progression of the ictal wavefront across the cortex (Schevon *et al*., 2012), as persistent HFOs only appear after the ictal wavefront has passed through the area.

Another difference between the HFOs evident in the microelectrode and subdural recordings relates to their appearance in unfiltered signals. Whereas HFOs associated with ictal discharges were easily visually discriminated in all the microelectrode recordings (Fig. 2A), this was not always the case for the subdural EEG recordings (Supplementary Fig. 3). Certainly, the contribution of sharp transients to the high gamma band filtered signal is well understood (Urrestarazu *et al*., 2007; Bénar *et al*., 2010), although by itself it cannot explain many of the observed HFOs. It is important to recognize that the variable visual presentation of HFOs in a prolonged train of epileptiform discharges does not detract from classifying the site as core territory, as long as at least some of the HFOs can be confirmed in the unfiltered signal. The consistency of our findings with the definitive site classification afforded by the microelectrode recordings provides substantial support for this position. Furthermore, analyses based on filtered high gamma amplitude or power have been previously used to identify ictal activity (David *et al*., 2011; Gnatkovsky *et al*., 2011; Wykes *et al*., 2012), albeit without the 'gold standard' validation available in our study.

Mapping seizure core territories

Much animal work has shown intense bursts of action potentials riding on the crest of a synaptically driven depolarization, referred

to as a paroxysmal depolarizing shift (Goldensohn and Purpura, 1963; Traub *et al*., 1993; Grenier *et al*., 2003), coordinated in all local neurons by the rhythmic synaptic onslaught. Because synaptic barrages flash across the recording area of a subdural electrode at high speed, with lags across a 4 mm distance of only a few milliseconds (Schevon *et al*., 2012), the multi-unit firing bursts overlap to a great extent. This is the basis of the observed 'hyper-synchronization' of multi-unit firing in the ictal core. Multi-unit activity and high gamma peak amplitudes are then coupled to the phase of the lower frequency dominant ictal rhythm, producing an oscillatory hierarchy analogous to that which has been described in macaque sensory cortices under normal conditions (Lakatos *et al*., 2005, 2008). Thus, HFOs in the ictal core mirror the intense, widespread neuronal firing during a narrow time window that may be regarded as the 'output' corresponding to the 'input' of the excitatory synaptic activity that is evident in low frequency signals. In contrast, in the penumbral territory this translation from synaptic 'input' to neuronal firing 'output' is blocked by the inhibitory veto mechanism (Trevelyan *et al*., 2006, 2007). Thus, the penumbra is marked by weak cross-frequency coupling, and consequently by low-level and minimally fluctuating high gamma amplitude in recordings from large surface (subdural) electrodes.

The term 'ictal core' refers to the region that has been invaded by the seizure, as evidenced by signature neural activity. This distinguishes it from the 'seizure onset zone', which is traditionally presumed to be the origination site of the seizure, but is in practice defined as the area in which low frequency ictal discharges initially appear and spread. As noted above, synaptic activity is distributed very rapidly and may extend quite some distance from its source, resulting in an apparent area that is larger than the ictal core. Thus, the seizure onset zone would be expected to include both core and penumbral territories. Currently, the proportion of the seizure onset zone that is penumbral, or that is invaded only late in the seizure and thus may be spared resection, is unknown. Subject to the limitations of subdural electrode coverage and grid resolution, we can estimate the true extent of the ictal core using the specific type of HFO that we have associated with ictal core activity.

The PLHG measure enables us to extrapolate the features of the ictal core demonstrated by our spatially restricted microelectrode data onto broader subdural electrode recordings. The PLHG measure is more efficient than standard techniques for HFO detection, and has the additional advantage of discounting HFOs that are less likely to be generated by synchronized pyramidal neuron bursting. The resulting maps of the presumptive ictal core territory and its trajectory of spread reveal a picture of seizure evolution that is at odds with the appearance in wideband EEG or extracellular recordings, and that bear out several predictions from our earlier analysis of multi-unit activity in the small (16 mm^2) area sampled by the microelectrode array.

The location of the ictal core within the first few seconds after initiation of (PLHG) recruitment lay within the boundaries of the clinically-determined seizure onset zone in all cases (with the exception of a single electrode site in Patient D, who had an Engel III outcome after multiple subpial transections). Later in the seizure, the expansion of the core included areas outside the seizure onset zone. This was particularly true for Patient A, in whom secondary generalization occurred ~25 s after seizure onset. The extent of the core increased sharply following the time of the clinical transition but did not encompass all recording sites (Fig. 8B and G). This interesting observation is consistent with observations from ictal SPECT studies, demonstrating increased perfusion in subcortical structures including the thalamus, and decreased perfusion in the cortical 'default mode network' (Blumenfeld *et al*., 2009). The sharp expansion of core recruited areas may be the result of increased excitatory thalamocortical activity.

We observed sharp spatial gradients in the PLHG measure in adjacent (1 cm spaced) subdural electrodes, even though the low frequency signals in the same electrodes appeared remarkably similar (Fig. 7). In cases where the microelectrode array was located in penumbral territory, we suspected that ictal core territory lay nearby based on clinical considerations. All microelectrode implant sites were within the seizure onset zone, and Patient C was seizure-free (2 year follow-up) after resection of a relatively small (3 × 3 cm) region encompassing both the PLHG-identified channels and the microelectrode implant site. We indeed found that in both penumbral recording cases, the ictal core was located within 1 cm of the implant site. These observations highlight the abrupt transition in neural activity between core and penumbra territories (Fig. 3). We previously reported that the ictal wavefront separating the two regions is quite narrow, <1.5 mm (Schevon *et al*., 2012).

We had hypothesized, based on the slow speed (<1 mm/s) of ictal wavefront propagation and the fact that signature ictal neural firing has only rarely been detected in humans despite many recording attempts (Wyler, 1982; Babb *et al*., 1987; Truccolo *et al*., 2011; Bower *et al*., 2012; Schevon *et al*., 2012), that the ictal core is far smaller in extent than has been traditionally suspected based on low frequency EEG interpretation. Our small study seems to confirm this hypothesis: the ictal core was found to comprise only 17% of the total seizure territory as judged by a measure designed to approximate the results of visual EEG interpretation. Further, the rate at which new channels were incorporated into the presumptive ictal core territory (0.5 per second) is consistent with the measured pace of seizure propagation (<1 mm/s) noted in our earlier study (Schevon *et al*., 2012), and in slice models with inhibition preserved (Trevelyan *et al*., 2007), given the 1 cm interelectrode spacing in the subdural arrays and that the measured rate reflects expansion of the ictal core to surrounding subdural electrode sites in multiple directions simultaneously. The rate is also consistent with the measured pace of clinical symptom progression during a Jacksonian march (Jasper, 1969).

Our analysis revealed that the rate of ictal core expansion was far more stereotypical than was true of the extent of EEG low frequency activity. This finding lends additional support to our contention that the seizure is being driven from the ictal core, and that penumbral activity is a secondary effect.

Conclusion

It has been known for many years that the seizure onset zone usually overlaps with the cortical regions generating high rates of

ictal high frequency oscillations (Fisher *et al*., 1992; Alarcon, 1995; Worrell *et al*., 2004). Here we have provided an explanation for this association that has immediate importance not only for clinical management, as well as a practical method of identifying the presumptive ictal core. Without a clearly defined distinction between the ictal core and penumbral territories, basic investigations into questions such as epileptogenesis and seizure prediction will necessarily be hampered. From a clinical standpoint, the ability to pinpoint the seizure core regions promises to improve the management of focal seizures, either by minimizing the volume of tissue resections (Ochi *et al*., 2007; David *et al*., 2011; Modur *et al*., 2011; Fujiwara *et al*., 2012; Park *et al*., 2012; Schevon *et al*., 2012), or by identifying new resection targets that have previously been overlooked. Alternatively, new treatments such as closed loop stimulation (Berenyi *et al*., 2012) or focal gene therapy (Wykes *et al*., 2012) may have improved efficacy if they are targeted accurately.

Acknowledgements

We would like to thank the treating epileptologists and fellows at Columbia University Medical Centre: Carl Bazil, Frank Gilliam, Lawrence Hirsch, Anil Mendiratta, Alison Pack, Steven Karceski, Derek Chong, Hyunmi Choi, Peter Tai, Alfred Frontera, Sara Inati, Elizabeth Gerard, and Daniel Friedman. We would especially like to thank the study patients, whose contribution and selfless participation are deeply appreciated. The authors would like to thank Charles Schroeder, Sameer Seth, and Chad Carlson for helpful comments on earlier drafts of the manuscript.

Funding

Funded by the National Institutes of Health (NINDS K08 NS48871, CAS, R25 10416928, S.A.W.), Epilepsy Research UK (A.J.T.), and the UK Medical Research Council (A.J.T.).

Supplementary material

Supplementary material is available at *Brain* online.

References

Alarcon G. Power spectrum and intracranial EEG patterns at seizure onset in partial epilepsy. Electroencephalogr Clin Neurophysiol 1995; 94: 326–37.

Babb TL, Wilson CL, Isokawa-Akesson M. Firing patterns of human limbic neurons during stereoencephalography (SEEG) and clinical temporal lobe seizures. Electroencephalogr Clin Neurophysiol 1987; 66: 467–482.

Bénar CG, Chauvière L, Bartolomei F, Wendling F. Pitfalls of high-pass filtering for detecting epileptic oscillations: a technical note on "false" ripples. Clin Neurophysiol 2010; 121: 301–10.

Berenyi A, Belluscio M, Mao D, Buzsaki G. Closed-loop control of epilepsy by transcranial electrical stimulation. Science 2012; 337: 735–7.

Blumenfeld H, Varghese GI, Purcaro MJ, Motelow JE, Enev M, McNally KA, et al. Cortical and subcortical networks in human secondarily generalized tonic-clonic seizures. Brain 2009; 132: 999–1012.

Bower MR, Stead M, Meyer FB, Marsh WR, Worrell GA. Spatiotemporal neuronal correlates of seizure generation in focal epilepsy. Epilepsia 2012; 53: 807–16.

Bragin A, Mody I, Wilson CL, Engel J Jr. Local generation of fast ripples in epileptic brain. J Neurosci 2002; 22: 2012–21.

Busse L, Wade AR, Carandini M. Representation of concurrent stimuli by population activity in visual cortex. Neuron 2009; 64: 931–42.

Canolty RT, Edwards E, Dalal SS, Soltani M, Nagarajan SS, Kirsch HE, et al. High gamma power is phase-locked to theta oscillations in human neocortex. Science 2006; 313: 1626–8.

Cohen-Gadol AA, Wilhelmi BG, Collignon F, White JB, Britton JW, Cambier DM, et al. Long-term outcome of epilepsy surgery among 399 patients with nonlesional seizure foci including mesial temporal lobe sclerosis. J. Neurosurgery 2006; 104: 513–24.

David O, Blauwblomme T, Job AS, Chabardès S, Hoffmann D, Minotti L, et al. Imaging the seizure onset zone with stereo-electroencephalography. Brain 2011; 134: 2898–911.

Dzhala VI, Staley KJ. Mechanisms of fast ripples in the hippocampus. J Neurosci 2004; 24: 8896–906.

Engel J Jr, Bragin A, Staba R, Mody I. High-frequency oscillations: what is normal and what is not? Epilepsia 2009; 50: 598–604.

Esteller R, Echauz J, Tcheng T, Litt B, Pless B. Line length: an efficient feature for seizure onset detection. IEEE 2001; 1707–10.

Fisher RS, Webber WR, Lesser RP, Arroyo S, Uematsu S. High-frequency EEG activity at the start of seizures. J Clin Neurophys 1992; 9: 441–8.

Foffani G, Uzcategui YG, Gal B, Menendez de la Prida L. Reduced spike-timing reliability correlates with the emergence of fast ripples in the rat epileptic hippocampus. Neuron 2007; 55: 930–41.

Fujiwara H, Greiner HM, Lee KH, Holland-Bouley KD, Seo JH, Arthur T, et al. Resection of ictal high-frequency oscillations leads to favorable surgical outcome in pediatric epilepsy. Epilepsia 2012; 53: 1607–17.

Gnatkovsky V, Francione S, Cardinale F, Mai R, Tassi L, Russo Lo G, et al. Identification of reproducible ictal patterns based on quantified frequency analysis of intracranial EEG signals. Epilepsia 2011; 52: 477–88.

Goldensohn ES, Purpura DP. Intracellular potentials of cortical neurons during focal epileptogenic discharges. Science 1963; 139: 840–2.

Grenier F, Timofeev I, Steriade M. Neocortical very fast oscillations (ripples, 80–200 Hz) during seizures: intracellular correlates. J Neurophysiol 2003; 89: 841–52.

Jacobs J, LeVan P, Chander R, Hall J, Dubeau F, Gotman J. Interictal high-frequency oscillations (80-500 Hz) are an indicator of seizure onset areas independent of spikes in the human epileptic brain. Epilepsia 2008; 49: 1893–907.

Jacobs J, Staba R, Asano E, Otsubo H, Wu JY, Zijlmans M, et al. High-frequency oscillations (HFOs) in clinical epilepsy. Prog Neurobiol 2012; 98: 302–15.

Jeha LE, Najm I, Bingaman W, Dinner D, Widdess-Walsh P, Lüders H. Surgical outcome and prognostic factors of frontal lobe epilepsy surgery. Brain 2007; 130: 574–84.

Jasper HH. Mechanisms of propagation: extracellular studies. In: Jasper HH, Ward AA, Pope A, editors. Basic mechanisms of the epilepsies, including hippocampus. Boston: Little, Brown; 1969.

Jirsch JD. High-frequency oscillations during human focal seizures. Brain 2006; 129: 1593–608.

Lakatos P, Karmos G, Mehta AD, Ulbert I, Schroeder CE. Entrainment of neuronal oscillations as a mechanism of attentional selection. Science 2008; 320: 110–3.

Lakatos P, Shah AS, Knuth KH, Ulbert I, Karmos G, Schroeder CE. An oscillatory hierarchy controlling neuronal excitability and stimulus processing in the auditory cortex. J Neurophysiol 2005; 94: 1904–11.

Le Van Quyen M, Bragin A, Staba R, Crépon B, Wilson CL, Engel J Jr. Cell type-specific firing during ripple oscillations in the hippocampal formation of humans. J. Neurosci 2008; 28: 6104–10.

Menendez de la Prida L, Trevelyan AJ. Cellular mechanisms of high frequency oscillations in epilepsy: on the diverse sources of pathological activities. Epilepsy Res 2011; 97: 308–17.

Modur PN, Zhang S, Vitaz TW. Ictal high-frequency oscillations in neocortical epilepsy: implications for seizure localization and surgical resection. Epilepsia 2011; 52: 1792–801.

Ochi A, Otsubo H, Donner EJ, Elliott I, Iwata R, Funaki T, et al. Dynamic changes of ictal high-frequency oscillations in neocortical epilepsy: using multiple band frequency analysis. Epilepsia 2007; 48: 286–96.

Park SC, Lee SK, Che H, Chung CK. Ictal high-gamma oscillation (60-99 Hz) in intracranial electroencephalography and postoperative seizure outcome in neocortical epilepsy. Clin Neurophysiol 2012; 123: 1100–10.

Penny WD, Duzel E, Miller KJ, Ojemann JG. Testing for nested oscillation. J Neurosci Methods 2008; 174: 50–61.

Prince DA, Wilder BJ. Control mechanisms in cortical Epileptogenic Foci* 'Surround' inhibition. Arch Neurol 1967; 16: 194–202.

Ray S, Crone NE, Niebur E, Franaszczuk PJ, Hsiao SS. Neural correlates of high-gamma oscillations (60-200 Hz) in macaque local field potentials and their potential implications in electrocorticography. J Neurosci 2008; 28: 11526–36.

Ray S, Maunsell J. Different origins of gamma rhythm and high-gamma activity in macaque visual cortex. PloS Biol 2011; 9: e10000610.

Rosenow F, Lüders H. Presurgical evaluation of epilepsy. Brain 2001; 124: 1683–700.

Schauerte B, Fink GA. Focusing computational visual attention in multimodal human-robot interaction. New York: ACM Press; 2010. p. 1.

Scheffer-Teixeira R, Belchior H, Leao RN, Ribeiro S, Tort ABL. On high-frequency field oscillations (>100 Hz) and the spectral leakage of spiking activity. J Neurosci 2013; 33: 1535–9.

Schevon CA, Weiss SA, McKhann G Jr, Goodman RR, Yuste R, Emerson RG, et al. Evidence of an inhibitory restraint of seizure activity in humans. Nat Commun 2012; 3. 1060.

Schindler K, Leung H, Elger CE, Lehnertz K. Assessing seizure dynamics by analysing the correlation structure of multichannel intracranial EEG. Brain 2007; 130: 65–77.

Schomburg EW, Anastassiou CA, Buzsáki G, Koch C. The spiking component of oscillatory extracellular potentials in the rat hippocampus. J Neurosci 2012; 32: 11798–811.

Staba R, Wilson C, Bragin A, Fried I, Engel J. Quantitative analysis of high-frequency oscillations (80-500 Hz) recorded in human epileptic hippocampus and entorhinal cortex. J Neurophysiol 2002; 88: 1743–52.

Traub RD, Miles R, Jefferys JG. Synaptic and intrinsic conductances shape picrotoxin-induced synchronized after-discharges in the guinea-pig hippocampal slice. J Physiol 1993; 461: 525–47.

Trevelyan AJ, Sussillo D, Watson BO, Yuste R. Modular propagation of epileptiform activity: evidence for an inhibitory veto in neocortex. J Neurosci 2006; 26: 12447–55.

Trevelyan AJ, Sussillo D, Yuste R. Feedforward inhibition contributes to the control of epileptiform propagation speed. J Neurosci 2007; 27: 3383–7.

Trevelyan AJ. The direct relationship between inhibitory currents and local field potentials. J Neurosci 2009; 29: 15299–307.

Truccolo W, Donoghue JA, Hochberg LR, Eskandar EN, Madsen JR, Anderson WS, et al. Single-neuron dynamics in human focal epilepsy. Nat Neurosci 2011; 14: 635–41.

Urrestarazu E, Chander R, Dubeau F, Gotman J. Interictal high-frequency oscillations (100-500 Hz) in the intracerebral EEG of epileptic patients. Brain 2007; 130: 2354–66.

Wetjen NM, Marsh WR, Meyer FB, Cascino GD, So E, Britton JW, et al. Intracranial electroencephalography seizure onset patterns and surgical outcomes in nonlesional extratemporal epilepsy. J Neurosurgery 2009; 110: 1147–52.

Worrell G, Parish L, Cranstoun S, Jonas R, Baltuch G, Litt B. High-frequency oscillations and seizure generation in neocortical epilepsy. Brain 2004; 127: 1496–506.

Wykes RC, Heeroma JH, Mantoan L, Zheng K, MacDonald DC, Deisseroth K, et al. Optogenetic and potassium channel gene therapy in a rodent model of focal neocortical epilepsy. Sci Transl Med 2012; 4: 161ra152.

Wyler A. Neuronal activity during seizures in monkeys. Exp Neurol 1982; 76: 574–85.

Ylinen A, Bragin A, Nádasdy Z, Jandó G, Szabó I, Sik A, et al. Sharp wave-associated high-frequency oscillation (200 Hz) in the intact hippocampus: network and intracellular mechanisms. J Neurosci 1995; 15: 30–46.